Exploiting Known Resonance Structure of Lipids for Improved Nuisance Removal from ^{1}H-MRSI Data

Qiang Ning[1,2], Fan Lam[1], Chao Ma[1,3,4],Bryan Clifford[1,2], and Zhi-Pei Liang[1,2]

[1] Beckman Institute for Advanced Science and Technology, University of Illinois at Urbana-Champaign, IL

[2] Department of Electrical and Computer Engineering, University of Illinois at Urbana-Champaign, IL

[3] Gordon Center for Medical Imaging, Massachusetts General Hospital, MA

[4] Department of Radiology, Harvard Medical School, MA

Running title: Exploiting Known Resonance Structure of Lipid for ^{1}H-MRSI Nuisance Removal

Submission category: Note

Correspondence to:

Qiang Ning
Beckman Institute for Advanced Science and Technology
405 N. Mathews Ave, Urbana, IL 61801 USA
E-mail: qning2@illinois.edu

Approximate word count for the manuscript body: 26xx words.

ABSTRACT

Purpose: To exploit the known resonance structures of lipid (and water) signals for improved nuisance removal from ^{1}H-MRSI data.

Methods: The proposed method uses the resonance structures of water and lipid molecules to construct a parametric model for the nuisance signals and combines it with the union-of-subspaces (UoSS) nuisance removal framework. Specifically, this parametric model is used to estimate the water and lipid signals, which are used to estimate the subspaces for the water and lipid signals, respectively. The estimated subspaces are then incorporated in the UoSS framework for improved nuisance removal performance.

Results: The proposed method was validated using three-dimensional MRSI data collected from the brain using an FID sequence with short-TE and no suppression pulses from healthy subjects. Improvement in reducing the level of nuisance signals using the proposed method compared to the original UoSS method was observed without any noticeable distortion to the desired metabolite spectra. Moreover, a subspace-based spatiospectral reconstruction was also performed to further demonstrate the effectiveness of the proposed nuisance removal method.

Conclusion: The known resonance structures of nuisance signals are useful prior knowledge that can be exploited for nuisance removal. Using this knowledge, the proposed method can effectively remove the overwhelming nuisance signals from ^{1}H-MRSI data collected with neither water nor lipid suppression pulses, which is desirable for optimizing ^{1}H-MRSI data acquisition.

Keywords

spectroscopic imaging, resonance structure, nuisance removal, non-suppression pulses

INTRODUCTION

^{1}H-MRSI is a promising tool for early detection and diagnosis of various diseases by providing metabolic information non-invasively (1–3), but its practical use has long been limited by the challenges of effective removal of the overwhelming water and lipid signals (a.k.a. nuisance signals). Various methods have been proposed to tackle this problem, including nuisance suppression techniques during data acquisition (4–12) and post-processing methods (13–21), by exploiting the differences between nuisance and desirable metabolite signals in terms of resonance frequency, relaxation time, and spatial support.

In this work, we aim to further exploit the resonance structures of the nuisance components (especially of lipid) for improved ^{1}H-MRSI nuisance removal. It has been shown that the major component of MR measurable subcutaneous lipid is triglyceride (22, 23), which has a well-defined resonance structure as shown in Table 1. By exploiting this resonance structure, one could expect: i) a better representation of the nuisance signals (and thus a cleaner removal) and ii) a better separation of the nuisance signals from the desired metabolite signals (and thus a better protection of metabolites). While the resonance structures of nuisance signals were used in various studies (24–27), explicitly using this readily available prior knowledge for nuisance removal has not yet been investigated to the best of our knowledge.

Our early attempt to use the resonance structures was reported in (28), where a generalized-series (GS) (29) is used to compensate any local line-shape distortions caused by field inhomogeneity, which results in a large, computationally expensive nonlinear optimization problem. In this work, we propose to use the resonance structures to construct a parametric model for the water and lipid signals; the nuisance subspace structures are then determined and incorporated into the union-of-subspaces (UoSS) nuisance removal framework for nuisance removal (21). The effectiveness of this proposed method has been demonstrated using experimental data acquired from healthy subjects on a 3 Tesla Siemens Trio MRI scanner. As we show later, incorporating known resonance structure allows the temporal sampling of MRSI signals to be below the Nyquist rate and as well as the elimination of the suppression pulses, both of which are desirable for MRSI data acquisition design. To further demonstrate the performance of the estimated subspace structure in protecting metabolite signals, a recent subspace-based reconstruction method (32, 33) was also performed to demonstrate the metabolic information obtained.

THEORY

UoSS Modeling

As described in the UoSS approach in (21), for practical applications of ^{1}H-MRSI, there exist strong spatiotemporal or spatiospectral correlations in the water and lipid components in the high-dimensional function $\rho(\mathbf{x}, t)$. Therefore, $\rho(\mathbf{x}, t)$ can be represented by the following UoSS model.[1]

$$\rho(\mathbf{x}, t) = \sum_{l=1}^{L_F} u_l^F(\mathbf{x}) v_l^F(t) + \sum_{l=1}^{L_W} u_l^W(\mathbf{x}) v_l^W(t), \quad [1]$$

where $\{v_l^I(t)\}_{l=1}^{L_I}$, I = {"F", "W"} are the sets of temporal bases spanning the low-dimensional subspaces that the water and lipid signals reside in and $\{u_l^I(\mathbf{x})\}_{l=1}^{L_I}$, I = {"F", "W"} are the corresponding spatial coefficients. The letters "F" and "W" stand for lipid (fat) and water, respectively. We can see from Eq. [1] that the UoSS modeling can lead to low-rank matrix representations that reduce the degrees of freedom of nuisance signal significantly and thus, allows effective removal of nuisance from limited or sparsely sampled k-space data with the capability of incorporating other prior information (21).

Resonance Structures of Nuisance Signals

The resonance structures of different molecules are known to significantly improve the spectral estimation of metabolites (34–37). Since nuisance removal can also be viewed as a spectral estimation problem (for nuisance components), the resonance structure of nuisance components may also help improve nuisance removal and can be incorporated besides the subspace constraints. The resonance structure of water is well-known to be a singlet at 4.7 ppm; the resonance structure of triglycerides (main component of MR measurable lipids (22, 23)) is a bit more complicated and shown in Table 1, where each of the resonance peak represents a structurally distinct proton moiety in a triglyceride molecule. As the level of saturation usually varies, ratios among different triglyceride peaks are usually not known a priori (25) (unlike the situation of metabolite quantification). In addition, no correlation has been observed between the line-widths of individual peaks of triglycerides (24). Therefore, the peaks shown in Table 1 should be treated individually. Specifically, we invoke the following

[1] Here we have assumed that we can approximate $\rho(\mathbf{x}, t)$ using water and lipid signals only, given the fact that the magnitude of metabolite signals is much lower than nuisance signals.

parametric model for the quantification of water and lipid spectroscopic signal:

$$\rho_W(\mathbf{x}_q, t_p; \mathbf{\Theta}_q^W) = a_q^W e^{-\frac{t_p}{T_{2,q}^W} - j2\pi f_q^W}, \quad [2]$$

$$\rho_F(\mathbf{x}_q, t_p; \mathbf{\Theta}_q^F) = \sum_{k=1}^{K} a_{q,k}^F e^{-\frac{t_p}{T_{2,q,k}^F} - j2\pi f_{q,k}^F}, \quad [3]$$

where water and lipid spectra are modeled by a sum of Lorentzian shapes with the chemical shifts of water and lipid shown in Table 1, and $\mathbf{\Theta}_q^I = \{\mathbf{a}_q^I, \mathbf{T}_{2,q}^I\}$, I = {"F", "W"} are the sets of spectral parameters for voxel $\mathbf{x}_q$. In the next, we describe how to integrate the spectral constraints in Eqs. [2] and [3] into the subspace constraints proposed in UoSS for improved nuisance removal.

Exploitation of Resonance Structures in UoSS

The UoSS model in Eq. [1] exploits the fact that each signal component lives in a low-dimensional subspace (21, 31) and a key issue for nuisance removal using UoSS is to determine the temporal bases of the subspace. To this end, the model in Eqs. [2] and [3] allows us to quantify water and lipid and retrieve temporal bases from the estimated water and lipid signals. Assuming the discretized spatiotemporal signals $d(\mathbf{x}, t)$, $\mathbf{x} = \mathbf{x}_1, \ldots, \mathbf{x}_Q$, $t = t_1, \ldots, t_P$, have already been reconstructed from the (k,t)-space data, we propose to solve the following optimization problem:

$$\hat{\mathbf{\Theta}}_q^W, \hat{\mathbf{\Theta}}_q^F, \Delta\hat{f}_q = \arg \min_{\mathbf{\Theta}_q^W, \mathbf{\Theta}_q^F, \Delta f_q} \sum_{p=1}^{P} |d(\mathbf{x}_q, t_p) - \left[\rho_W(\mathbf{x}_q, t_p; \mathbf{\Theta}_q^W) + \rho_F(\mathbf{x}_q, t_p; \mathbf{\Theta}_q^F)\right] e^{j2\pi\Delta f_q t_p}|^2, \quad [4]$$

for $q = 1, \ldots, Q$, where Δf_q is the field inhomogeneity at $\mathbf{x}_q$. The problem in Eq. [4] is a typical quantification problem with both nonlinear and linear parameters, which can be solved using the variable projection method (38, 39). Using the estimated spectral parameters (i.e., $\hat{\mathbf{\Theta}}_q^W$ and $\hat{\mathbf{\Theta}}_q^F$), we can synthesize water and lipid signals based on Eqs. [2] and [3] and get $\hat{\rho}_W(\mathbf{x}_q, t_p)$ and $\hat{\rho}_F(\mathbf{x}_q, t_p)$. Then the temporal bases for water and fat, $\{v_l^W(t)\}_{l=1}^{L_W}$ and $\{v_l^F(t)\}_{l=1}^{L_F}$, can be extracted as the dominant singular vectors of the Casorati matrices

$$\mathbf{C}^I(\boldsymbol{\rho}) = \begin{bmatrix} \hat{\rho}_I(\mathbf{x}_1, t_1) & \hat{\rho}_I(\mathbf{x}_2, t_1) & \cdots & \hat{\rho}_I(\mathbf{x}_Q, t_1) \\ \hat{\rho}_I(\mathbf{x}_1, t_2) & \hat{\rho}_I(\mathbf{x}_2, t_2) & \cdots & \hat{\rho}_I(\mathbf{x}_Q, t_2) \\ \vdots & \vdots & \ddots & \vdots \\ \hat{\rho}_I(\mathbf{x}_1, t_P) & \hat{\rho}_I(\mathbf{x}_2, t_P) & \cdots & \hat{\rho}_I(\mathbf{x}_Q, t_P) \end{bmatrix}, \; I = \{\text{"W"}, \text{"F"}\}, \quad [5]$$

In addition, since field inhomogeneity can also be obtained from quantification, a separate acquisition for field map is not required.

Estimation of Nuisance Signals

Once the temporal bases (denoted by $\{\hat{v}_l^W(t)\}_{l=1}^{L_W}$ and $\{\hat{v}_l^F(t)\}_{l=1}^{L_F}$) are determined, the nuisance removal problem is to determine their corresponding spatial coefficients from MRSI measurement in the (k,t)-space, which can be modeled follows.

$$d(\mathbf{k},t) = \int \rho(\mathbf{x},t) e^{j2\pi\Delta f(\mathbf{x})t} e^{-j2\pi\mathbf{k}\mathbf{x}} d\mathbf{x} + n(\mathbf{k},t), \quad [6]$$

where thermal noise $n(\mathbf{k},t)$ follows a white Gaussian distribution and $\rho(\mathbf{x},t)$ can be represented by

$$\rho(\mathbf{x},t) = \sum_{q=1}^{Q} \rho(\mathbf{x}_q,t)\varphi_q(\mathbf{x}), \quad [7]$$

where $\varphi_q(\mathbf{x})$ can be chosen as a 3D rectangular function for the q-th voxel. Then we have

$$d(\mathbf{k},t) \;=\; w(\mathbf{k}) \sum_{q=1}^{Q} \rho(\mathbf{x}_q,t) e^{j2\pi\Delta f(\mathbf{x}_q)t} e^{-j2\pi\mathbf{k}\mathbf{x}_q} + n(\mathbf{k},t), \quad [8]$$

where $w(\mathbf{k}) = \int \varphi(\mathbf{x}) e^{-j2\pi\mathbf{k}\mathbf{x}} d\mathbf{x}$ and the sum over q can be computed efficiently by the fast Fourier transform (FFT) algorithm. Finally, by re-writing the UoSS model in Eq. [1] and the imaging model in Eq. [8] in a more compact matrix-form, we propose to estimate spatial coefficients by solving the optimization problem below.

$$\hat{\mathbf{U}} = \arg\min_{\mathbf{U}} \|\mathbf{d} - \mathbf{\Omega_k W F}\{\mathbf{\Omega_x U}\hat{\mathbf{V}}^T \odot \hat{\mathbf{B}}\}\|_2^2 + \lambda\|\mathbf{U}\|_F^2, \quad [9]$$

where $\mathbf{d}$ is to put $d(\mathbf{k},t)$ into a vector, $\mathbf{\Omega_k}$ is the data sampling mask in k-space, $\mathbf{W}$ represents the weighting factor $w(\mathbf{k})$, $\mathbf{F}$ represents FFT from x-space to k-space, $\mathbf{\Omega_x} = \text{diag}\{\mathbf{\Omega}_\mathbf{x}^W, \mathbf{\Omega}_\mathbf{x}^F\}$ is the spatial support for water and fat, $\mathbf{U} = [\mathbf{U}_W, \mathbf{U}_F]$ contains the spatial coefficients to be estimated, $\hat{\mathbf{V}} = \left[\hat{\mathbf{V}}_W, \hat{\mathbf{V}}_F\right]$ contains the estimated temporal bases by stacking $\{\hat{v}_l^W(t)\}_{l=1}^{L_W}$ and $\{\hat{v}_l^F(t)\}_{l=1}^{L_F}$ column-wisely, and $\hat{\mathbf{B}}$ models the field inhomogeneity effects, i.e., $\hat{\mathbf{B}}(\mathbf{x}_q,t_p) = e^{j2\pi\Delta\hat{f}_q t_p}$. The problem in Eq. [9] is a linear least squares problem with Tikhonov regularization and thus can be readily solved using the conjugate descent method, and the value of λ can be selected using the discrepancy principle (40). The estimated nuisance signals can then be represented by the UoSS model using $\hat{\mathbf{U}}$ and $\hat{\mathbf{V}}$ and removed from MRSI data.

METHODS

In Vivo Experiments

In vivo data were collected from healthy volunteers on a 3T Siemens Trio scanner (Siemens Healthcare) equipped with a 12-channel headcoil. The study was approved by the local Institutional Review Board. For

each subject, a high-resolution 3D ^{1}H-MRSI dataset was acquired in a 7.6-minute scan using a gradient-echo based EPSI sequence with the following imaging parameters: FOV = 230 mm $\times$ 230 mm $\times$ 72 mm, excitation slab thickness = 60 mm, elliptically sampled spatial encoding matrix = 76 $\times$ 76 $\times$ 24 (i.e., 3 mm isotropic nominal resolution), TR/TE =310/4 ms, flip angle = 43°, echo spacing = 1.66 ms, number of echoes per TR = 128 (flyback acquisition), readout bandwidth = 125kHz. Two saturation bands were used to suppress signals outside the FOV along the slice selective direction. A five-minute 3D magnetization prepared rapid gradient echo (MP RAGE) (41) scan at 0.9 mm isotropic resolution was acquired for anatomical reference information. In addition, a two-minute low-resolution 3D ^{1}H-MRSI dataset was acquired in order to retrieve metabolite basis for SPICE using the same sequence and imaging parameters, except that: spatial encoding matrix = 16 $\times$ 16 $\times$ 12, echo spacing = 0.66 ms, number of echoes per TR = 600 (bipolar acquisition), readout bandwidth = 68 kHz, signal average = 2, weak water suppression using WET pulses (7) and eight OVS bands surround the brain for fat suppression (8).

Data Processing

For nuisance removal, the MP RAGE images were first aligned with the high-resolution 3D MRSI data and segmented using SPM8 (42) to obtain spatial supports of fat and water. The proposed quantification with water and lipid in Eq. [4] exploiting resonance structure was then performed to obtain field inhomogeneity $\Delta\hat{f}(\mathbf{x})$ and temporal bases $\hat{\mathbf{V}}$, followed by the estimation of spatial coefficients $\hat{\mathbf{U}}$ in Eq. [9]. An extra step is further used to locally handle the residual nuisance signals that cannot be predicted perfectly by the UoSS model due to practical issues such as large B_0 inhomogeneity, partial volume effect, and subject head motion. To be precise, the extra step incorporates a convolution kernel in the frequency domain to the estimated water signals to account for peak distortions (as is done similarly in LCModel (34)).

After nuisance signal removal, metabolite subspaces were estimated from the low-resolution 3D MRSI data, with which high-resolution metabolite signals were reconstructed from the nuisance removed data using SPICE described in (32, 33, 43). Both the nuisance signal removal and SPICE reconstruction were performed in a coil-by-coil fashion followed by SVD-based combination to form the final spatiotemporal reconstruction (44).

RESULTS

Figure 1 compares the normalized projection errors of signals from the subcutaneous layer onto the subspaces estimated by the HSVD method used in original UoSS (21) (solid line) and by the proposed method exploiting resonance structures (dashed line). Both the two subspaces include the same set of water bases to account for water signals in the subcutaneous region so that Fig. 1 is focused on comparing the effects of different numbers of lipid bases. We can see as the number of lipid bases increases, both two curves decrease as expected. Moreover, the dashed line is consistently lower than the solid line, especially when the number of bases is less than 20, which indicates that the representation of lipid signals using the subspace estimated by exploiting resonance structures is more effective. Therefore, in practice, the proposed method allows the use of a lower model order for lipid in nuisance removal, which provides us more computational efficiency and potentially better metabolite protection.

Figure 2 shows the nuisance removal effect from one high-resolution 3D MRSI acquisition without suppression pulses, where the images of ℓ_2 spectral integral corresponding to only one of the phased-array coils are shown. Specifically, Fig. 2a is the unsuppressed MRSI signal; Fig. 2b is the residual after applying Papoulis-Gerchberg (PG) algorithm (45, 46) for removing signals lying in the subcutaneous layer and HSVD (13) for removing water components; Fig. 2c is the residual after applying the original UoSS method (21); and Fig. 2d and Fig. 2e are the residual signals after exploiting resonance structures of nuisance components in UoSS and the extra local removal step, respectively. We can see in Fig. 2b that the Gibbs ringing of lipid and residual water were still very large; the UoSS method significantly improved nuisance removal, but there were still noticeable residual signals, especially in the subcutaneous layer (Fig. 2c), which was further improved by the proposed subspace estimation method (Fig. 2d); finally, the proposed local removal step reduced any residual nuisance signals at voxels with strong spectral distortion to a negligible level (Fig. 2e). Note when performing the original UoSS method and the proposed removal method, same number of water and lipid bases were used. Therefore, the proposed physics-derived subspace estimation has the capability of better representing nuisance signals with a lower model order.

Figure 3 shows the ℓ_2 norm and some representative spectra of the nuisance removed data after a truncation in k-space for better SNR. Specifically, the residual after the proposed local removal step is truncated in the k-space from $76\times76\times24$ to $16\times16\times12$ with a hamming window applied. From the spatial distribution and representative spectra in Fig. 3, we can see that the desired metabolite signals are well-preserved without

significant contamination caused by residual nuisance signals.

Figure 4 summarizes the various information that can be retrieved from the high-resolution MRSI data collected without suppression pulses, including field inhomogeneity and T_2^* mapping. More importantly, with the help of the proposed nuisance removal method and an extra training dataset (required by SPICE), very rich spectral/metabolic information can be obtained at a high-resolution and high-SNR using SPICE, which is very appealing for various MRSI studies.

CONCLUSION

This note investigates the use of known resonance structures of nuisance signals (especially of lipids) for improved nuisance removal. More specifically, the known resonance structures were used to derive the subspace representation for the water and lipid signals, which were then used in the union-of-subspaces framework for nuisance removal. The effectiveness of the proposed method has been demonstrated using in vivo short-TE ^{1}H-MRSI data acquired without suppression pulses. The proposed method may provide new flexibility for ^{1}H-MRSI acquisition.

ACKNOWLEDGMENTS

This work was supported in part by the National Institutes of Health; Grant numbers: NIH-1RO1-EB013695 and NIH-R21EB021013-01.

References

1. Gonen O, Oberndorfer TA, Inglese M, Babb JS, Herbert J, Grossman RI, Reproducibility of three whole-brain N-acetylaspartate decline cohorts in relapsing-remitting multiple sclerosis. AJNR Am J Neuroradiol 2007;28:267–271.

2. Gomes WA, Lado FA, de Lanerolle NC, Takahashi K, Pan C, Hetherington HP, Spectroscopic imaging of the pilocarpine model of human epilepsy suggests that early NAA reduction predicts epilepsy. Magn Reson Med 2007;58:230–235.

3. Posse S, Otazo R, Dager SR, Alger J, MR spectroscopic imaging: Principles and recent advances. J Magn Reson Imaging 2013;37:1301 – 1325.

4. Haase A, Frahm J, Hanicke W, Matthaei D, ^{1}H NMR chemical shift selective (CHESS) imaging. Phys Med Biol 1985;30:341–344.

5. Bydder G, Steiner R, Blumgart L, MR imaging of the liver using short T_1 inversion recovery. J Comput Assist Tomogr 1985;9:1084–1089.

6. Spielman DM, Pauly JM, Macovski A, Glover GH, Enzmann DR, Lipid-suppressed single-and multisection proton spectroscopic imaging of the human brain. J Magn Reson Imaging 1992;2:253–262.

7. Ogg R, Kingsley R, Taylor J, WET, a T1- and B1-insensitive water-suppression method for in vivo localized ^{1}H NMR spectroscopy. J Magn Reson Series B 1994;104:1 – 10.

8. Le Roux P, Gilles R, McKinnon G, Carlier P, Optimized outer volume suppression for single-shot fast spin-echo cardiac imaging. J Magn Reson Imaging 1998;8:1022–1032.

9. de Graaf RA, Nicolay K, Adiabatic water suppression using frequency selective excitation. Magn Reson Med 1998;40:690–696.

10. Luo Y, De Graaf R, DelaBarre L, Tannus A, Garwood M, BISTRO: An outer-volume suppression method that tolerates RF field inhomogeneity. Magn Reson Med 2001;45:1095–1102.

11. Ebel A, Govindaraju V, Maudsley AA, Comparison of inversion recovery preparation schemes for lipid suppression in ^{1}H MRSI of human brain. Magn Reson Med 2003;49:903–908.

12. Andronesi OC, Gagoski BA, Sorensen AG, Neurologic 3D MR spectroscopic imaging with low-power adiabatic pulses and fast spiral acquisition. Radiology 2012;262:647–661.

13. Barkhuisen H, de Beer R, van Ormondt D, Improved algorithm for noniterative time-domain model fitting to exponentially damped magnetic resonance signals. J Magn Reson 1987;73:553 – 557.

14. Hu X, Patel M, Chen W, Ugurbil K, Reduction of truncation artifacts in chemical-shift imaging by extended sampling using variable repetition time. J Magn Reson Series B 1995;106:292–296.

15. Haupt CI, Schuff N, Weiner MW, Maudsley AA, Removal of lipid artifacts in ^{1}H spectroscopic imaging by data extrapolation. Magn Reson Med 1996;35:678–687.

16. Metzger G, Sarkar S, Zhang X, Patel KHM, Hu X, A hybrid technique for spectroscopic imaging with reduced truncation artifact. Magn Reson Imaging 1999;17:435–443.

17. Sarkar S, Heberlein K, Hu X, Truncation artifact reduction in spectroscopic imaging using a dual-density spiral k-space trajectory. Magn Reson Imaging 2002;20:743–757.

18. Dong Z, Hwang JH, Lipid signal extraction by SLIM: application to ^{1}H MR spectroscopic imaging of human calf muscles. Magn Reson Med 2006;55:1447–1453.

19. Hernando D, Haldar J, Sutton B, Liang ZP, Removal of lipid signal in MRSI using spatial-spectral constraints. In: *Proc IEEE Int Symp Biomed Imaging*, Arlington, VA, USA, 2007; pp. 1360–1363.

20. Bilgic B, Gagoski B, Kok T, Adalsteinsson E, Lipid suppression in CSI with spatial priors and highly undersampled peripheral k-space. Magn Reson Med 2013;69:1501–1511.

21. Ma C, Lam F, Johnson CL, Liang ZP, Removal of nuisance signals from limited and sparse ^{1}H MRSI data using a union-of-subspaces model. Magn Reson Med 2015;.

22. Brix G, Heiland S, Bellemann M, Koch T, Lorenz W, MR imaging of fat-containing tissues: valuation of two quatitative imaging techniques in comparison with localized proton spectroscopy. Magn Reson Med 1993;11:977–991.

23. Ren J, Dimitrov I, Sherry A, Malloy C, Composition of adipose tissue and marrow fat in humans by ^{1}H NMR at 7 Tesla. J Lipid Res 2008;49:2055–2062.

24. Hamilton G, Middleton MS, Bydder M, Yokoo T, Schwimmer JB, Kono Y, Patton HM, Lavine JE, Sirlin CB, Effect of PRESS and STEAM sequences on magnetic resonance spectroscopic liver fat quantification. J Magn Reson Imaging 2009;30:145–152.

25. Hamilton G, Yokoo T, Bydder M, Cruite I, Schroeder M, Sirlin C, Middleton M, In vivo characterization of the liver fat ^{1}H MR spectrum. NMR Biomed 2011;24:784–790.

26. Thomsen C, Becker U, Winkler K, Christoffersen P, Jensen M, Henriksen O, Quantification of liver fat using magnetic resonance spectroscopy. Magn Reson Imaging 1994;12:487–495.

27. Hernando D, Kellman P, Haldar J, Liang Z, Robust water/fat separation in the presence of large field inhomogeneities using a graph cut algorithm. Magn Reson Med 2010;63:79–90.

28. Ning Q, Ma C, Lam F, Clifford B, Liang ZP, Removal of nuisance signal from sparsely sampled ^{1}H-MRSI data using physics-based spectral bases. In: *Proc of the Int Symp Magn Reson Med*, Singapore, 2016; .

29. Liang ZP, Lauterbur PC, A generalized series approach to MR spectroscopic imaging. IEEE Trans Med Imag 1991;10:132 – 137.

30. Liang ZP, Spatiotemporal imaging with partially separable functions. In: *IEEE International Symposium on Biomedical Imaging*, Arlington, VA, USA, 2007; pp. 988 – 991.

31. Clifford B, Ma C, Lam F, Liang ZP, Removal of nuisance signals from limited and sparse 3D ^{1}H-MRSI data of the brain. In: *Proc of the International Symposium on Magnetic Resonance in Medicine*, Toronto, Canada, 2015; p. 984.

32. Lam F, Liang ZP, A subspace approach to high–resolution spectroscopic imaging. Magn Reson Med 2014; 71:1349 – 1357.

33. Lam F, Ma C, Clifford B, Johnson CL, Liang ZP, High-resolution ^{1}H-MRSI of the brain using SPICE: data acquisition and image reconstruction. Magn Reson Med 2015;.

34. Provencher SW, Estimation of metabolite concentrations from localized in vivo proton NMR spectra. Magn Reson Med 1993;30:672–679.

35. Ratiney H, Sdika M, Coenradie Y, Cavassila S, van Ormondt D, Graveron-Demilly D, Time-domain semi-parametric estimation based on a metabolite basis set. NMR Biomed 2005;18:1–13.

36. Poullet JB, Sima DM, Simonetti AW, de Neuter B, Vanhamme L, Lemmerling P, van Huffel S, An automated quantitation of short echo time MRS spectra in an open source software environment: AQSES. NMR Biomed 2007;20:493–504.

37. Ning Q, Ma C, Liang ZP, Spectral estimation for magnetic resonance spectroscopic imaging with spatial sparsity constraints. In: *Proc IEEE Int Symp Biomed Imaging*, 2015; pp. 1482–1485.

38. Golub GH, Pereyra V, The differentiation of pseudo-inverses and nonlinear least squares problems whose variables separate. SIAM J Numer Anal 1973;10.

39. Van der Veen JWC, De Beer R, Luyten P, Van Ormondt D, Accurate quantification of in vivo ^{31}P NMR signals using the variable projection method and prior knowledge. Magn Reson Med 1988;6:92–98.

40. Vogel CR, *Computational methods for inverse problems*. Philadelphia, PA: SIAM, 2002.

41. Brant-Zawadzki M, Gillan GD, Nitz WR, MP RAGE: a three-dimensional, T1-weighted, gradient-echo sequence–initial experience in the brain. Radiology 1992;182:769–775.

42. Friston KJ, Holmes AP, Worsley KJ, Poline JP, Frith CD, Frackowiak RS, Statistical parametric maps in functional imaging: a general linear approach. Human Brain Mapping 1994;2:189–210.

43. Ma C, Lam F, Ning Q, Johnson CL, Liang ZP, High-resolution ^{1}H-MRSI of the brain using short-TE SPICE. Magn Reson Med 2016;.

44. Bydder M, Hamilton G, Yokoo T, Sirlin C, Optimal phased-array combination for spectroscopy. Magn Reson Imag 2008;26:847–850.

45. Gerchberg R, Super-resolution through error energy reduction. J Mod Optic 1974;21:709–720.

46. Papoulis A, A new algorithm in spectral analysis and band-limited extrapolation. Circuits and Systems, IEEE Transactions on 1975;22:735–742.

47. Bydder M, Girard O, Hamilton G, Mapping the double bonds in triglycerides. Magn Reson Imag 2011; 29:1041–1046.

Table 1: MR Resonance Structure of Water and Triglycerides (25, 47)

Chemical Shift (ppm)	Assignment	Type
4.7	$\mathbf{H}_2$O	Water
5.29	-C**H**=CH-	Olefinic
5.19	-C**H**-O-CO-	Glycerol
4.2	-C$\mathbf{H}_2$-O-CO-	Glycerol
2.75	-CH=CH-C$\mathbf{H}_2$-CH=CH-	Diacyl
2.20	-CO-C$\mathbf{H}_2$-CH_2-	α-Carboxyl
2.02	-C$\mathbf{H}_2$-CH=CH-C$\mathbf{H}_2$-	α-Olefinic
1.6	-CO-CH_2-C$\mathbf{H}_2$-	β-Carboxyl
1.3	-(C$\mathbf{H}_2$)$_n$-	Methylene
0.9	-$(CH_2)_n$-C$\mathbf{H}_3$-	Methyl

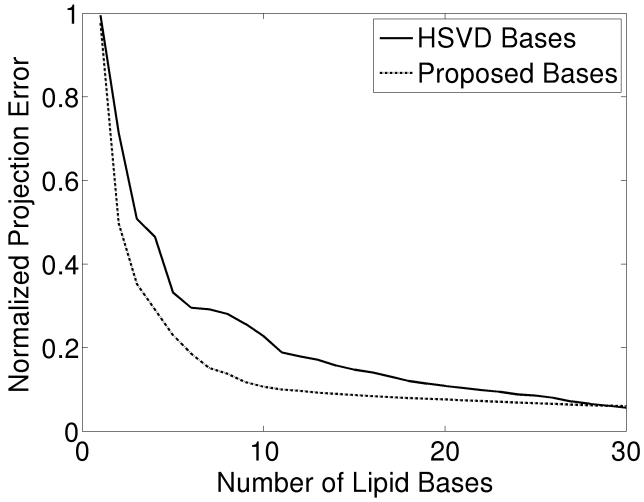

Figure 1: Comparison of the projection errors of lipid signals onto the subspaces obtained by HSVD in (21) (solid line) and the proposed method (dashed line), respectively. We can see that the dashed line is consistently lower than the solid line (i.e., more accurate representation), especially when the number of lipid bases is small.

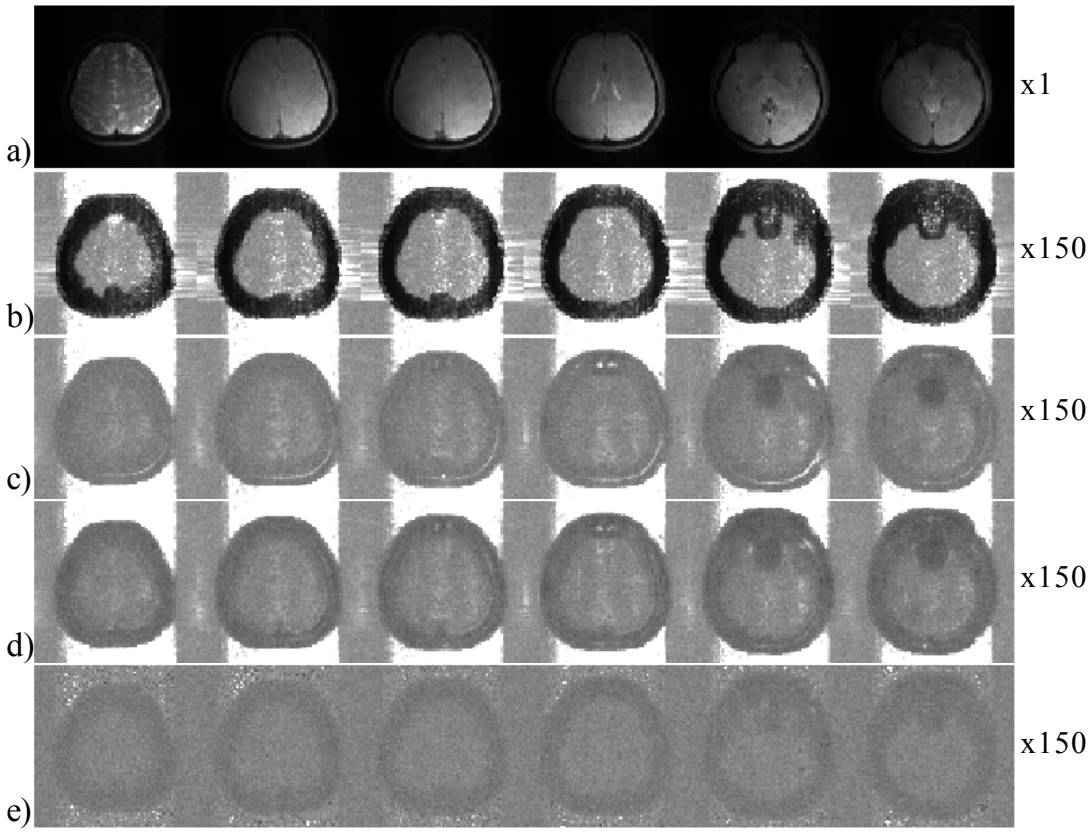

Figure 2: The spectral integral of a) the original unsuppressed MRSI signals from one coil and the corresponding residual signals after nuisance removal using b) PG and HSVD, c) the original UoSS method, d) and e) the proposed nuisance removal before and after the extra local removal step, respectively. Same number of water and lipid bases were used for both c) and d). Note the negligible level of nuisance signals in e) except for some isolated outer-brain regions.

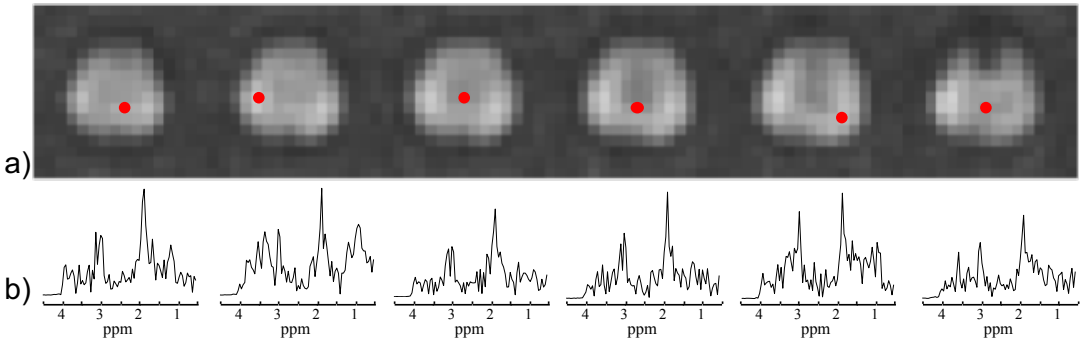

Figure 3: Illustration of the capability of the proposed method in protecting metabolite signals. a) The spectral integral of the nuisance removed data after truncation in k-space from $76\times76\times24$ to $16\times16\times12$. b) Spectra from several representative locations, which are marked in red dots in a).

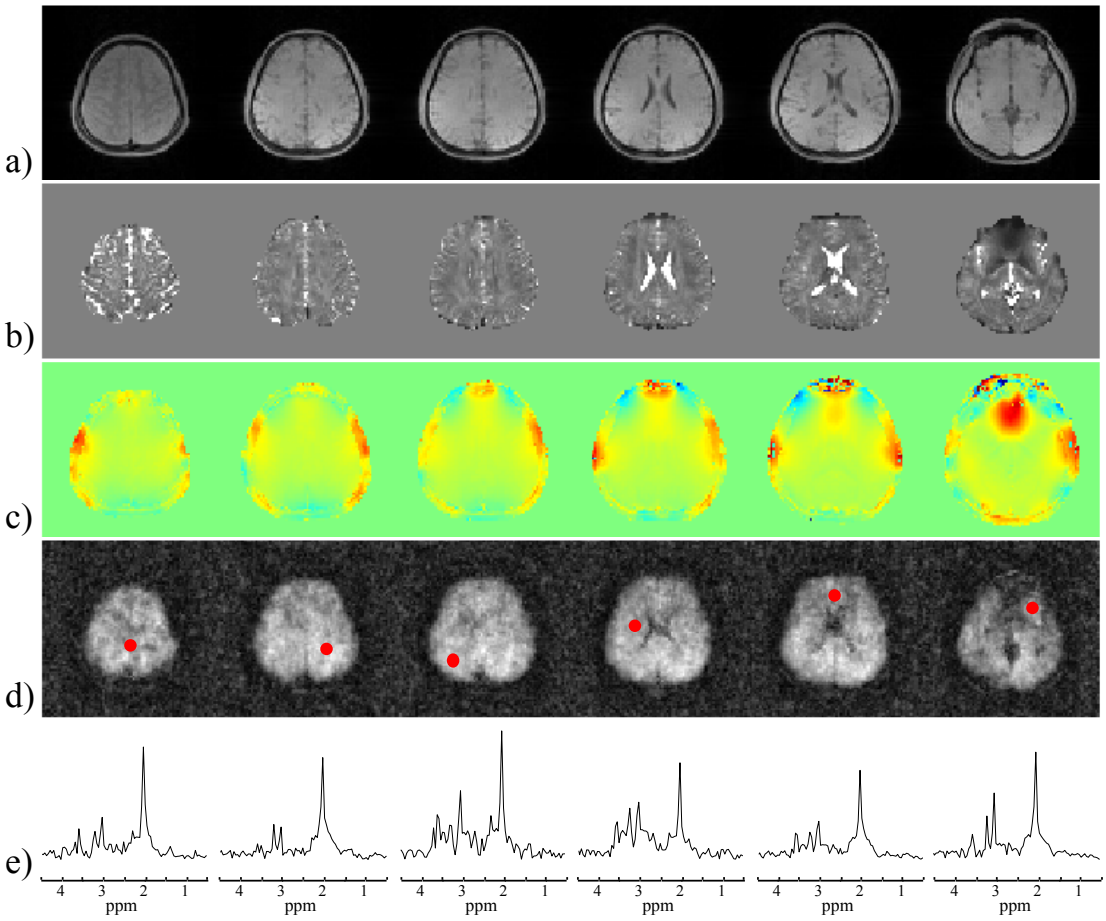

Figure 4: Various information that can be obtained within a ten-minute MRSI scan (one 7.6-minute high-resolution dataset and one two-minute low-resolution training dataset), enabled by the proposed nuisance removal method for unsuppressed MRSI data: a) water images, b) T_2^* maps, c) field inhomogeneity maps from the companion water signals, d) the NAA maps obtained from the nuisance removed data using SPICE, and e) representative spectra from the marked locations in d).